Smooth periodic gauge satisfying crystal symmetry and periodicity to study high-harmonic generation in solids

Shicheng Jiang,[1,2] Chao Yu,[1] Jigen Chen,[3] Yanwei Huang,[2] Ruifeng Lu,[1,*] and C. D. Lin[4,†]

[1]*Institute of Ultrafast Optical Physics, Nanjing University of Science and Technology, Nanjing 210094, People's Republic of China*

[2]*State Key Laboratory of Precision Spectroscopy, East China Normal University, Shanghai 200062, People's Republic of China*

[3]*Zhejiang Provincial Key Laboratory for Cutting Tools, Taizhou University, Taizhou 31800, People's Republic of China*

[4]*J. R. Macdonald Laboratory, Department of Physics, Kansas State University, Manhattan, Kansas 66506, USA*

(Received 13 March 2020; accepted 24 September 2020; published 12 October 2020)

Intense lasers can easily drive nonadiabatic transitions of excited electron wave packets across the Brillouin zones, thus transition dipole moments (TDM) between energy bands of solids should be continuous, satisfying crystal symmetry, and periodic at zone boundaries. While current *ab initio* algorithms are powerful in calculating band structures of solids, they all introduced random phases into the eigenfunctions at each crystal momentum $\boldsymbol{k}$. Here we show how to choose a "smooth-periodic" gauge where TDMs can be smooth versus $\boldsymbol{k}$, preserving crystal symmetry, as well as maintaining periodic at boundaries. The symmetry properties of TDMs with respect to $\boldsymbol{k}$ ensure the absence of even-order harmonics from MgO with inversion symmetry, while the TDM in the "smooth-periodic" gauge for broken-symmetry ZnO is responsible for even harmonics that were underestimated in previous simulations. These results reveal the importance of correctly treating the complex TDMs that satisfy crystal symmetry and continuous across zone boundaries in nonlinear laser-solid interactions, which has been elusive in most theories so far.

DOI: 10.1103/PhysRevB.102.155201

I. INTRODUCTION

In quantum mechanics, band theory is the foundation for understanding the structure of solids and their interactions with lights. To interpret a plethora of experiments on all kinds of condensed materials, *ab initio* computer codes have been developed and the values of such packages are well recognized. In recent years, with the advent of intense lasers and their nonlinear interactions with solids, ultrafast phenomena like high-order harmonic generation (HHG) [1–5], laser-induced charge transfer [6–10], Bloch oscillation [11–13], laser-controlled dielectrics [14,15], and ultrafast renormalization [16–18] have been widely investigated. The equations of motion based on band theory and crystal-momentum representation, for example, semiconductor Bloch equations (SBEs) [19–24] and other extended forms [25–27], have already been used to interpret these nonlinear ultrafast phenomena. The related theoretical methods were summarized in the review [28]. However, true quantitative comparison between theoretical results with experiments remains a challenge, despite that the band structure and transition dipoles were calculated from advanced *ab initio* codes.

In the interaction of strong lasers with solids, nonadiabatic transitions of electrons between bands are important, since the excited electron wave packet can even go across the first Brillouin zone. When the carrier is moving along a path in the $\boldsymbol{k}$ space, the wave packet will acquire a dynamical phase and a geometry phase [29,30]. Previously, the geometric phase was mostly considered only for closed paths to ensure the theory is gauge independent. However, as shown recently [31,32], in the SBE method for high-order harmonic generation in solids, gauge invariance is achieved when the correct phase of the transition dipole moment (TDM) is included in the SBEs. In principle, the combination of geometry phase and dipole phase is well-defined whether the system is open or closed [32]. Both of these two phases will be encoded in the macroscopic polarization, and thus the photonic signal [30].

In order to describe the interaction of strong laser fields with solids in a finite $\boldsymbol{k}$ space including the phase accumulated by the moving wave packet, it requires that (i) the TDMs should be calculated accurately for the whole first Brillouin zone; (ii) the TDMs with $\boldsymbol{k}$-dependent phase should be continuous and periodic with respect to k. Using *ab initio* software to calculate accurate absolute values of TDMs, Yu *et al.* [33] were able to obtain improved HHG spectra. However, since all *ab initio* algorithms calculated the eigenfunctions at each $\boldsymbol{k}$ separately, random phases are introduced at each k point and the phase of the TDM is not smooth and continuous. By noting the importance of the TDM phase, Jiang *et al.* [34] obtained the smooth phase analytically using the tight-binding model. They were able to reproduce the orientation dependence of the HHG spectra from ZnO reported by Ghimire *et al.* [1] and Gholam-Mirzaei *et al.* [2]. However, the tight-binding model is too primitive and there remains quantitative discrepancies with experiments. For accurate HHG theories, it is desirable to obtain an ambiguity-free phase for the TDM calculated from *ab initio* algorithms.

*rflu@njust.edu.cn
†cdlin@phys.ksu.edu

The problem of a random phase in TDM has been well recognized and studied for a long time [35–38] and solutions have been suggested there. The robust methods are step-by-step gauge transformation on the $\boldsymbol{k}$ grid [35] and utilizing basis constructed by symmetry-adapted maximally localized Wannier wave functions [39,40]. The latter has been included in the new release of WANNIER90 [41]. These two methods are noticed in the community of strong-field physics since the recent work from Ivanov's group [42]. The problem of a random phase can also be avoided by solving time-dependent Kohn-Sham equation in real space [43,44] or solving SBEs in velocity gauge [45]. In the previous works on solid HHG, the commonly used "smooth procedure" to fix the random phase in the $\boldsymbol{k}$ grid is the one suggested in Ref. [38]. This method will introduce Zak's phase [46] into the eigenfunctions and then break the periodicity of the TDMs which was also mentioned in Ref. [45]. In the present paper, we point out that this kind of "smooth procedure" is not robust, and is valid only for trivial systems [31,47].

In this paper we will obtain smooth TDM phase that also satisfies periodic conditions of the crystal by introducing what we will call the "smooth-periodic" gauge to distinguish it from the "periodic gauge". We first summarize the "smooth procedure", then address systems with and without inversion symmetry. In this "smooth-periodic" gauge, the symmetry properties of $\boldsymbol{k}$-dependent eigenfunctions and TDMs for system with inversion symmetry are retained. Such symmetry properties would ensure the absence of even-order harmonics driven by long pulses even if multiband excitations are included. Using such TDMs, we calculated the harmonic spectra of MgO and found improved agreement with earlier experiment. Similarly, we also revisited the HHG spectra of ZnO in the direction with broken symmetry. While even harmonics of ZnO were predicted by Jiang *et al.* [34], the signals were much too weak relative to the odd harmonics. With TDMs calculated using the "smooth-periodic" gauge, the even harmonics were greatly enhanced and become comparable to odd harmonics.

II. THE COMMONLY USED "SMOOTH PROCEDURE" AND ITS DEFICIENCY

It is necessary to show this method briefly here. The Bloch wave function is expressed as $\Phi_m(k,r) = e^{ikr}u_m(k,r)$ where $u_m(k,r)$ is periodic $u_m(k,r) = u_m(k,r+R)$, with R being the lattice spacing. In most *ab initio* software, the periodic part is expanded by plane waves $u_m(k,r) = \sum_h a(k+G_h)e^{iG_h r}$. In principle, the Bloch functions are periodic in $\boldsymbol{k}$ space $\Phi_m(k,r) = \Phi_m(k+G,r)$. Here, G is the reciprocal lattice vector. The eigenfunctions are obtained separately for different $\boldsymbol{k}$ points, which leads to random phases $\varphi_m(k)$, $u'_m = u_m(k,r)e^{i\varphi_m(k)}$. Note that $\varphi_m(k)$ is randomly generated and is discrete with respect to $\boldsymbol{k}$.

In the "smooth procedure", a complex number $z_m(k)$ is defined by

$$z_m(k) = |z_m(k)|e^{i\alpha_m(k)} = \langle u'_m(k,r)|u'_m(k+\Delta k,r)\rangle. \quad (1)$$

A new wave function is constructed by

$$u''_m(k+\Delta k,r) = u'_m(k+\Delta k,r)e^{-i\alpha_m(k)}. \quad (2)$$

By renaming the function $u''_m(k+\Delta k,r)$ according to

$$u''_m(k+\Delta k,r) \to u'_m(k+\Delta k,r), \quad (3)$$

the same procedure can be repeated with the next point $u'_m(k+2\Delta k,r)$. When this procedure goes over the first Brillouin zone, the phase-modified wave function become continuous with respect to $\boldsymbol{k}$. We rename the final wave function after the "smooth procedure" as $u^s_m(k,r)$ to distinguish it from the original one generated by *ab initio* software. The detail of the "smooth procedure" can also be found in Ref. [38] by Hjelm and coworkers.

Since Δk is small,

$$\langle u'_m(k,r)|u'_m(k+\Delta k,r)\rangle \approx e^{\Delta k\langle u_m(k,r)|\nabla_k u_m(k,r)\rangle + i(\varphi_m(k+\Delta k)-\varphi_m(k))}, \quad (4)$$

which leads to

$$u''_m(k+\Delta k,r) = u_m(k+\Delta k,r)e^{-\Delta k\langle u_m(k,r)|\nabla_k u_m(k,r)\rangle + i\varphi_m(k)}. \quad (5)$$

As the procedure of Eqs. (1)–(3) goes through the path $k_0 \to k_0 + k$, the phase-modified wave function becomes

$$u'_m(k,r) = u_m(k,r)e^{i\int_{k_0}^{k} dkD_{mm}(k)}e^{i\varphi_m(k_0)}, \quad (6)$$

where $D_{mm}(k) = i\langle u_m(k,r)|\nabla_k u_m(k,r)\rangle$ is the Berry connection.

To conclude, this method forces the wave function to be continuous with respect to $\boldsymbol{k}$, and the new Berry connection $D^s_{mm}(k) = i\langle u^s_m(k,r)|\nabla_k u^s_m(k,r)\rangle = 0$. Meanwhile, at the same time this method introduces a phase $\Theta_m(k) = \int_{k_0}^{k} d\kappa D_{mm}(\kappa) + \varphi_m(k_0)$ to the eigenfunction. The additional phase $\Theta_m(k)$ will break the periodicity of the eigenfunction. In the following two sections, we will provide different methods to deal with the nonperiodicity for systems with and without inversion symmetry.

III. SYSTEM WITH INVERSION SYMMETRY

The eigenfunction $u_m(k) = \sum_h a(k+G_h)e^{iG_h r}$ is defined in the "periodic gauge" [48]. As shown by Zak [46], the Zak's phase $\gamma = \int_k^{k+G} d\kappa D_{mm}(\kappa)$ is equal to zero or π in the "periodic gauge". Thus, for system with inversion symmetry, the simplest way for the "smooth procedure" is to extend it to the second Brillouin zone. In this way, phase difference between the starting point k_0 and $k_0 + 2G$ is zero or 2π, which means that the periodicity of eigenfunctions in $\boldsymbol{k}$ space is $2G$.

In this section, rocksalt MgO with inversion symmetry is taken as example to explain our method. Figure 1(b) shows the band structure of MgO along $(-1,0,-1) \to \Gamma(0,0,0) \to (1,0,1)$. Figures 1(c)–1(h) are the corresponding TDMs calculated by the "smooth procedure" between different pairs of bands. The eigenfunctions are calculated by the density functional theory (DFT) package in VASP [49] using the Perdew-Burke-Ernzeroff generalize gradient approximation functional. The cutoff energy of plane wave is 500 eV. Since the DFT simulation underestimates the band gap, the conduction bands are shifted to get better agreement with the experimental gap 7.8 eV. As expected, both the energy bands and TDMs are periodic with $2G$.

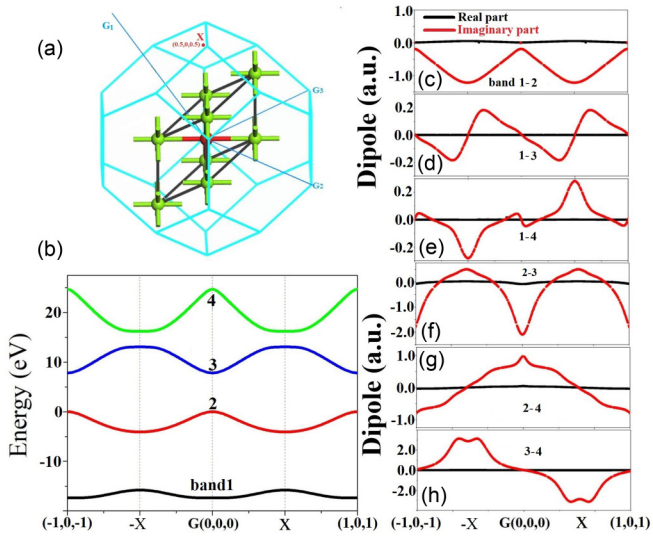

FIG. 1. (a) Geometric structure of rocksalt MgO crystal. Red and green balls are O and Mg, respectively. (b) Band structure along the Γ-X axis. (c)–(h) Real (black line) and imaginary (red line) part of TDMs generated by the "smooth procedure" in the extended Brillouin zone.

In Fig. 2, we present the HHG spectra calculated by solving SBEs with one valence band (band 2) and two conduction bands (band 3 and band 4) included. The spectra show two plateaus, with the right side of the dashed line being from the recombination of electron-hole pair from the second conduction band (band 4) to the valence band (band 2) [30]. To the left, which is due to recombination from band 3, the green arrow marks a minimum, which is similar to the Cooper minimum in atoms. Such a minimum originates from the minimum of the absolute value of the dipole moment between band 2 and band 3. This minimum has also been found in the time-dependent DFT simulation in Ref. [50]. Thus, it would be of interest to see if this minimum can be observed in experiments if the detected photon energy range can be extended [30,51,52]. This kind of minimum will be discussed in detail in another paper [53].

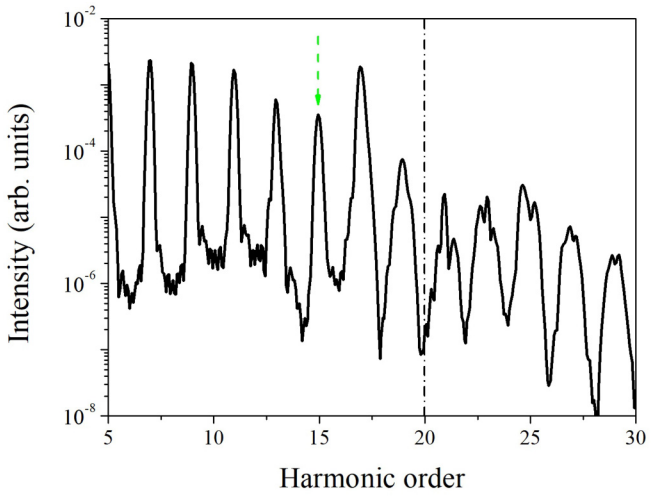

FIG. 2. HHG spectrum from MgO calculated by 1D three-band SBEs. The equations are solved in the extended Brillouin zone and all the elements used in the SBE model are from Fig. 1. Laser parameter: 30 fs, 1300 nm, 1×10^{13} W/cm^2.

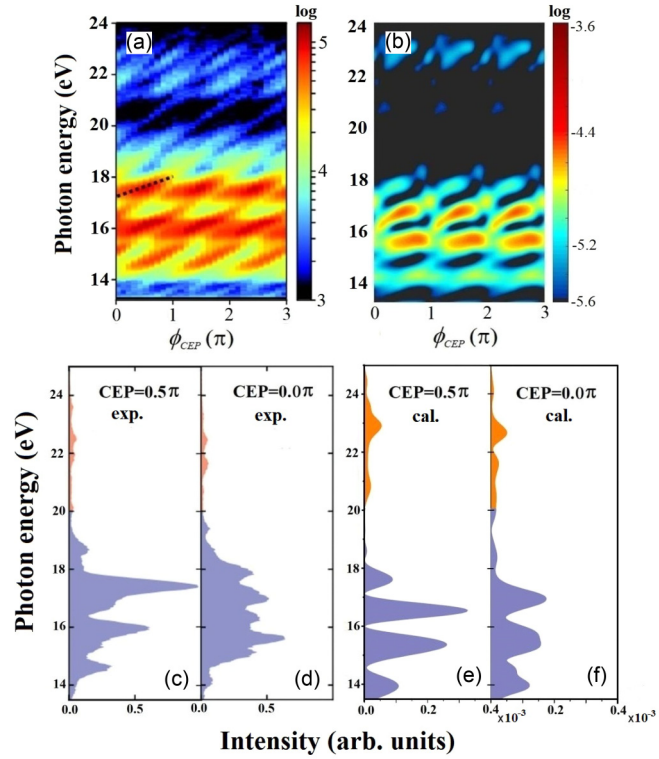

FIG. 3. Comparison between experimental and calculated CEP dependent HHG from MgO. (a), (c), and (d) are reprinted with permission from Ref. [30] ®. The Optical Society. (b), (e), and (f) are the calculated spectrum along Γ-X. Laser parameter: 1700 nm, 10 fs, 4×10^{13} W/cm^2.

From the analysis of Sec. II, after the "smooth procedure", the newly derived eigenfunction $u_m^s(k,r)$ satisfies the strict periodic boundary condition $u_m^s(k,r) = e^{i2Gr}u_m^s(k+2G,r)$ and $u_m^s(k,r) = e^{i2Gr}u_m^s(k,r+R)$. One still would like to know the symmetry properties of the TDMs for systems with inversion symmetry. The results are summarized in Table I while the derivation is given in the Appendix. When the periodic functions $u_m^s(k,r)$ and $u_n^s(k,r)$ have the same parity, the TDM between band m and n is an odd function with respect to k. When they have opposite parity, the TDMs between them is an even function with respect to k. In a three-band model, there are many pathways to generate excitations. Take the MgO example, one possibility is to choose a path *band* $2\rightarrow3\rightarrow4$. The corresponding macroscopic polarization is given by

$$\begin{aligned} P(t) &\sim P(k_0,t) + P(-k_0,t) \\ &= D_{24}(k_0+A(t))D_{43}(k_0+A(t))D_{32}(k_0+A(t))E(t)^2 \\ &\quad + D_{24}(-k_0+A(t))D_{43}(-k_0+A(t))D_{32}(-k_0+A(t))E(t)^2 \\ &\quad + \text{c.c.} \end{aligned} \tag{7}$$

Here $E(t)$ and $A(t)$ are electric field and vector potential, respectively. If the driven laser is a long pulse, $E(t+T/2) = -E(t)$ and $A(t+T/2) = -A(t)$, where T is the optical cycle

TABLE I. Properties of TDMs for different "parities" of eigenfunctions.

$u^s_m(k,r)$	$u^s_n(k,r)$	$D^s_{mn}(k)$
$u^s_m(-k,r)=u^s_m(k,-r)$	$u^s_n(-k,r)=u^s_n(k,-r)$	$D^s_{mn}(-k)=-D^s_{mn}(k)$
$u^s_m(-k,r)=u^s_m(k,-r)$	$u^s_n(-k,r)=-u^s_n(k,-r)$	$D^s_{mn}(-k)=D^s_{mn}(k)$
$u^s_m(-k,r)=-u^s_m(k,-r)$	$u^s_n(-k,r)=u^s_n(k,-r)$	$D^s_{mn}(-k)=D^s_{mn}(k)$
$u^s_m(-k,r)=-u^s_m(k,-r)$	$u^s_n(-k,r)=-u^s_n(k,-r)$	$D^s_{mn}(-k)=-D^s_{mn}(k)$

of the laser. Thus, we can get

$$\begin{aligned} P(t+T/2) &\sim P(k_0, t+T/2) + P(-k_0, t+T/2) \\ &= D_{24}(k_0 - A(t))D_{43}(k_0 - A(t))D_{32}(k_0 - A(t))E(t)^2 \\ &\quad + D_{24}(-k_0 - A(t))D_{43}(-k_0 - A(t))D_{32}(-k_0 - A(t))E(t)^2 \\ &\quad + \text{c.c.} \end{aligned} \tag{8}$$

By comparing Eqs. (7) and (8) and using the properties listed in Table I, we can find that $P(t) = -P(t+T/2)$ [the parities of the wave functions for these three bands are shown in Fig. 5(b)]. The odd parity of macroscopic polarization, similar to the case for an atomic target, guarantees that no even-order harmonics in the spectra. If the parities of TDMs have not accounted for, odd symmetric macroscopic polarization is not present. In other words, because of the parities of TDMs, coupling of multiple bands cannot generate even harmonics if the system has inversion symmetry.

Using the more accurate band structure and dipole moments, in particular, the new dipole phases constructed in the present "smooth-periodic" gauge, we can improve the simulation reported in Ref. [30] where the dipole moments have been set to be constant. Comparison of carrier-envelope-phase (CEP) dependent spectra between experimental data and our simulation is presented in Figs. 3(a) and 3(b). The laser parameters used in the simulation can be found in the caption. Many features in the experimental data are reproduced in the present simulation. (i) In Fig. 3(a), the slope of photon energy versus the CEP has been reproduced in Fig. 3(b). (ii) Both experiment and simulation show two plateaus, in the same photon energy region. (iii) In Fig. 3(b), our simulation indicates a minimum around 13 eV, which is consistent with experiment even though it is near the low energy end of the experimental data, thus it cannot be ruled out that the minimum is due to detector efficiency in the energy region. Note that this minimum also appears in Fig. 2 at the 15th order harmonic. Comparing with the simulations reported in Ref. [30], we have witnessed significant improvement in the present improved theory.

Figures 3(c)–3(f) compare the HHG spectra at two CEPs, $0.5\,\pi$ and 0.0, between experiment and the present simulation. It is clear that the sinelike pulse (CEP $= 0.5\,\pi$) would generate sharper discrete harmonics, while a cosinelike pulse would produce relatively flatter ones. Such results are in agreement with the measurements.

In this article, we are concerned with how harmonic spectra are affected if the parity and periodicity of transition dipole moments are not correctly accounted for. In many prior calculations, approximations were made in which the k-dependent dipole moments were taken to be its absolute values. This means that it is an even function with respect to k. In the three-band model for MgO, using the method presented here, $D_{c_1c_2}(k)$, which is the coupling between the two conduction bands, is an odd function. If we arbitrarily change it to an even function, how would the HHG spectra be altered? Figure 4 shows the original spectra copied from Fig. 3(c) (in black

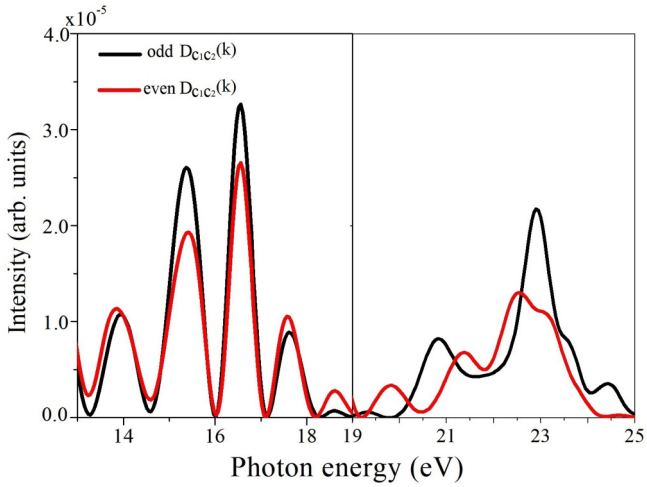

FIG. 4. HHG spectra from MgO using different TDMs. Black line is the same as Fig. 3(c): harmonic spectrum calculated using correct dipole moments [$D_{c_1c_2}(k)$ is odd, $D_{vc_2}(k)$] and $D_{vc_1}(k)$ are even functions of $\boldsymbol{k}$). Red line: The same as the black line except that $D_{c_1c_2}(k)$ is changed to an even function of $\boldsymbol{k}$ artificially. The subscripts v, c_1, c_2 represent the valence band, first conduction band and second conduction band, respectively. The intensities of the spectra in the right side of the vertical solid line were multiplied by a factor of 4.

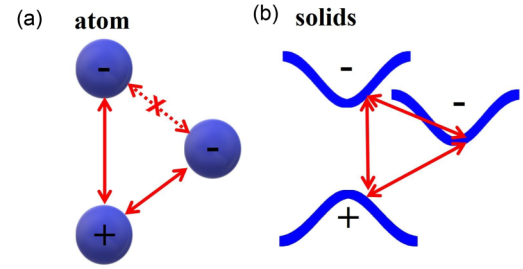

FIG. 5. Illustration of transition paths of electrons for gases and solids with inversion symmetry. For the gas phase, a triangular system will never be formed because transition between states with same parity is forbidden. For the solid case where the energy levels are extended into bands, transitions between bands at these k points away from Γ are not forbidden. The symmetry properties of the TDMs will ensure the absence of even order optical signal.

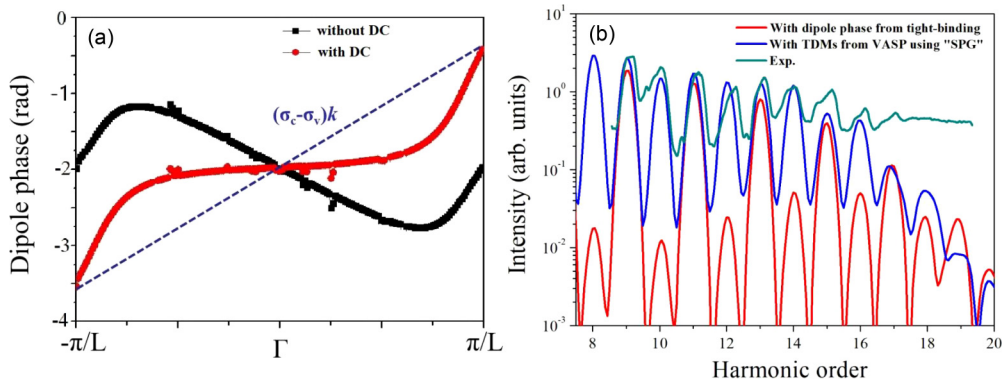

FIG. 6. Dipole phase of wurtzite ZnO crystal and simulated HHG. (a) Red line is the k-dependent dipole phase generated by "smooth procedure". Such a phase is not periodic because of the DC term in the additionally introduced phase. The black line is the k-dependent dipole phase after the DC component is taken away as introduced in this article. (b) HHG spectra from ZnO. The green line is the experimental data, the blue line is calculated by two-band SBEs with elements obtained from *ab initio* software with the help of the present "smooth-periodic" procedure. The red line is from calculations where the dipole phases are calculated from the tight-binding model. The red line and experimental data are copied from our previous work [34]. To present clear comparison, the spectra are shifted vertically.

lines) and compare it to HHG spectra (in red lines) if $D_{c_1c_2}(k)$ is changed to an even function. For the first plateau harmonics, no significant changes occur since the first plateau is due to recombination of electrons from the first conduction band to the valence band. For the harmonics in the second plateau, we can see the change as the harmonic peaks are shifted. Based on Eqs. (7), (8) and the analysis in Ref. [30], the peaks in the secondary plateau are given by $\omega = (2n - 1 - \theta/\pi)\omega_0$, where ω_0 is the frequency of the driving pulse and the phase θ is the phase difference between the two pathways to reach the conduction band 2. By changing the parity of $D_{c_1c_2}(k)$ artificially from odd to even, the peaks in the second plateau will be given by $\omega = (2n - \theta/\pi)\omega_0$. This can explain the shift of the peaks in the secondary plateau shown in Fig. 4. Thus, if the parity of the dipole moment has wrong parity, the generated harmonic spectra will be quite different.

We conclude this section by illustrating the difference between gas phase and solids, as shown in Fig. 5. In the gaseous medium with inversion symmetry, a triangular system will never be formed because of the parity of the wave function. For crystal with inversion symmetry where energy level is expanded into a band, a triangle system can be formed for k away from the Γ point, but the parity of the TDMs will prevent the generation of even-order harmonics.

IV. SYSTEM WITH BROKEN SYMMETRY

For system with broken symmetry, the Zak's phase can be any value. Thus, the method above for system with inversion symmetry is not valid anymore. Note that in the periodic gauge the Berry connection is periodic $D_{mm}(k) = D_{mm}(k + G)$, which means it can be expanded as

$$D_{mm}(k) = g_m(k) + \sigma_m, \tag{9}$$

where $g_m(k) = \sum_{n=1}^{+\infty} f_1(n)\cos(nLk) + f_2(n)\sin(nLk)$ is the "Alternating Current (AC)" component and σ_m is a constant which can be regarded as the "Direct Current (DC)" component. The DC component will lead to divergence of the introduced additional phase $\Theta_m(k) = \int_{k_0}^{k} d\kappa D_{mm}(\kappa) + \varphi_m(k_0)$. We do not need to care about the AC part, because this component would not influence the periodicity, the continuity, and the final observable physical quantities [27]. If the "smooth procedure" is carried out for the first Brillouin zone, the DC-induced nonperiodic phase of the TDMs between band m and n is $-(\sigma_m - \sigma_n)k$.

Here we take the direction Γ − A of wurtzite ZnO as an example. In Fig. 6(a), the red line is the k-dependent dipole phase for the first Brillouin zone obtained from VASP using a "smooth procedure". As stated above, the dipole phase cannot be ensured to be periodic because of the DC component. However, it is easy to get the slope by $-(\sigma_m - \sigma_n) = (\alpha_{mn}(\pi/L) - \alpha_{mn}(-\pi/L))/G$. Here, $\alpha_{mn}(\pm\pi/L)$ are the phase of TDMs, which are read from the data generated by the "smooth procedure" shown by the red line in Fig. 6(a). We can then get the periodic dipole phase by subtracting the DC part off

$$D^p_{mn}(k) = D^s_{mn}(k)e^{i(\sigma_m-\sigma_n)k} = D^s_{mn}(k)e^{-i(\alpha_{mn}(\pi/L)-\alpha_{mn}(-\pi/L))k/G}, \tag{10}$$

which is shown by the black line in Fig. 6(a) for ZnO. At the same time, the Berry connection is changed from zero to $D^p_{mm}(k) - D^p_{nn}(k) = \sigma_m - \sigma_n$. With that, all the elements in the SBE model are periodic and continuous with respect to k. This means that the equation of motion for carriers can be solved in a finite k space. In Fig. 6(b), the calculated HHG spectrum (blue line) by solving two-band SBE model using TDMs obtained by our "smooth-periodic" procedure is compared to the experimental data (green line). We also present the spectrum (red line) by solving two-band SBEs including only dipole phase obtained from the tight-binding model. Even though the tight-binding model can approximatively reproduce the orientation-dependent feature of HHG spectra, usually it is too primitive to produce the relative strength between odd and even order harmonics. Using accurate TDMs obtained from *ab initio* software with the help of our "smooth-periodic" procedure, the experimental spectra of ZnO reported in Ghimire *et al.* (1) has finally been satisfactorily reproduced theoretically.

V. CONCLUSION

Although *ab initio* software has been widely used to investigate electronic properties recently, the random phase generated in the algorithms prevents its application to calculate nonadiabatic dynamics, especially when the external field is a strong laser. In this article, we first show that the commonly used "smooth procedure" cannot ensure the periodicity of the wave function. Second, we provide two different methods to overcome this defect for systems with and without inversion symmetry. Because our approaches ensure continuity and periodicity of all the elements used in the equations of motion, the gauge resulting by the transformation of our methods can be referred to as a "smooth-periodic" gauge to distinguish it from "periodic" gauge used by Resta [48]. Based on this gauge, HHG spectra from solids with and without inversion symmetry are revisited. It is emphasized that symmetry properties are the key factors to ensure the absence of even order harmonics for systems with inversion symmetry. With the accurate TMDs with dipole phase and Berry connection, the HHG spectrum from ZnO with broken symmetry is also improved greatly. The TMDs introduced in this work is fundamental to all applications relating to optical signals from solids, such as laser wave-form control, band/dipole reconstruction, and detecting dynamic information. They should be used in any strong field theories for interpreting nonlinear interactions of laser lights with periodic materials.

ACKNOWLEDGMENTS

This work was supported by the NSF of China (11974185, 11704187, 11974112, 11975012) and the NSF of Jiangsu Province (Grant No. BK20170032). C.D.L. was supported in part by the Chemical Sciences, Geosciences, and Biosciences Division, Office of Basic Energy Sciences, Office of Science, U.S. Department of Energy, under Grant No. DE-FG02-86ER13491. S.J. is grateful for the support by the Project funded by China Postdoctoral Science Foundation No. 2019TQ0098. S.J. thanks Prof. C. Liu from the Beijing Institute of Technology and Dr. P. Saurabh from East China Normal University for fruitful discussions.

APPENDIX: DERIVATION OF THE PARITIES OF TRANSITION DIPOLE MOMENTS

Both $u_m^s(k,r)$ and $u_m^{kp}(k,r)$ satisfy the $k\cdot p$ equation,

$$\left(-\frac{1}{2}\nabla_r^2 + V(r) - ik\cdot\nabla_r\right)u_m^{s(kp)}(k,r) = \left(E_m(k) - \frac{k^2}{2}\right)u_m^{s(kp)}(k,r), \tag{A1}$$

where $u_m^{kp}(k,r)$ is assumed to satisfy

$$u_m^{kp}(-k,r) = u_m^{kp*}(k,r). \tag{A2}$$

When the system has inversion symmetry

$$u_m^{kp}(-k,r) = \pm u_m^{kp}(k,-r); \quad D_{mm}^{kp}(k) = 0, \tag{A3}$$

$u_m^s(k,r)$ must be related to $u_m^{kp}(k,r)$ through a gauge transformation, e.g.,

$$u_m^s(k,r) = u_m^{kp}(k,r)e^{i\beta(k)}. \tag{A4}$$

As stated in the main text, after the "smooth procedure", the Berry connection

$$D_{mm}^s(k) = i\langle u_m^s(k,r)|\nabla_k u_m^s(k,r)\rangle = 0. \tag{A5}$$

By inserting Eq. (A4) into Eq. (A5), we have

$$D_{mm}^s(k) = i\langle u_m^{kp}(k,r)e^{i\beta(k)}|\nabla_k\left(u_m^s(k,r)e^{i\beta(k)}\right)\rangle = D_{mm}^{kp}(k) - \nabla_k\beta(k). \tag{A6}$$

It is easy to prove that $D_{mm}^{kp}(k)$ is a real number and an even function with respect to k,

$$D_{mm}^{kp}(-k) = D_{mm}^{kp}(k). \tag{A7}$$

In order to ensure $D_{mm}^s(k) = 0$, $\beta(k) = odd\ function + const.$ Further, if the system has inversion symmetry, $\beta(k) = const.$ Thus, $u_m^s(k,r)$ also has

$$u_m^s(-k,r) = \pm u_m^{kp}(k,-r). \tag{A8}$$

Using Eq. (A8), we can get all the properties listed in Table I.

[1] S. Ghimire, A. D. DiChiara, E. Sistrunk, P. Agostini, L. F. DiMauro, and D. A. Reis, Nat. Phys. **7**, 138 (2011).
[2] S. Gholam-Mirzaei, J. Beetar, and M. Chini, Appl. Phys. Lett. **110**, 061101 (2017).
[3] G. Vampa, T. J. Hammond, N. Thiré, B. E. Schmidt, F. Légaré, C. R. McDonald, T. Brabec, and P. B. Corkum, Nature (London) **522**, 462 (2015).
[4] T. T. Luu, M. Garg, S. Yu. Kruchinin, A. Moulet, M. Th. Hassan, and E. Goulielmakis, Nature (London) **521**, 498 (2015).
[5] M. Hohenleutner, F. Langer, O. Schubert, M. Knorr, U. Huttner, S. W. Koch, M. Kira, and R. Huber, Nature (London) **523**, 572 (2015).
[6] A. Schiffrin, T. Paasch-Colberg, N. Karpowicz, V. Apalkov, D. Gerster, S. Mühlbrandt, M. Korbman, J. Reichert, M. Schultze, S. Holzner, J. V. Barth, R. Kienberger, R. Ernstorfer, V. S. Yakovlev, M. I. Stockman, and F. Krausz, Nature (London) **493**, 70 (2013).
[7] S. Yu. Kruchinin, M. Korbman, and V. S. Yakovlev, Phys. Rev. B **87**, 115201 (2013).
[8] T. Paasch-Colberg, A. Schiffrin, N. Karpowicz, S. Kruchinin, Ö. Sağlam, S. Keiber, O. Razskazovskaya, S. Mühlbrandt, A. Alnaser, M. Kübel, V. Apalkov, D. Gerster, J. Reichert, T. Wittmann, J. V. Barth, M. I. Stockman, R. Ernstorfer, V. S. Yakovlev, R. Kienberger, and F. Krausz, Nat. Photon. **8**, 214 (2014).
[9] G. Wachter, C. Lemell, J. Burgdörfer, S. A. Sato, X. M. Tong, and K. Yabana, Phys. Rev. Lett. **113**, 087401 (2014).
[10] S. C. Jiang, C. Yu. G. L. Yuan, T. Wu, Z. W. Wang, and R. F. Lu, J. Phys.: Condens. Matter **29**, 275702 (2017).
[11] O. Schubert, M. Hohenleutner, F. Langer, B. Urbanek, C. Lange, U. Huttner, D. Golde, T. Meier, M. Kira, S. W. Koch, and R. Huber, Nat. Photon. **8**, 119 (2014).
[12] L. Li, P. Lan, X. Liu, L. He, X. Zhu, O. D. Mücke, and P. Lu, Opt. Express **26**, 23844 (2018).

[13] L. Liu, J. Zhao, J. M. Yuan, and Z. X. Zhao, Chin. Phys. B **28**, 114205 (2019).

[14] M. Schultze, E. M. Bothschafter, A. Sommer, S. Holzner, W. Schweinberger, M. Fiess, M. Hofstetter, R. Kienberger, V. Apalkov, V. S. Yakovlev, M. I. Stockman, and F. Krausz, Nature (London) **493**, 75 (2013).

[15] M. Schultze, K. Ramasesha, C. D. Pemmaraju, S. Sato, D. Whitmore, A. Gandman, J. S. Prell, L. J. Borja, D. Prendergast, K. Yabana, D. M. Neumark, and S. Leone, Science **346**, 1348 (2014).

[16] A. Chernikov, C. Ruppert, H. M. Hill, A. F. Rigosi, and T. F. Heinz, Nat. Photon. **9**, 466 (2015).

[17] L. Meckbach, T. Stroucken, and S. W. Koch, Appl. Phys. Lett. **112**, 061104 (2018).

[18] L. Meckbach, J. Hader, U. Huttner, J. Neuhaus, J. T. Steiner, T. Stroucken, J. V. Moloneym, and S. W. Koch, Phys. Rev. B **101**, 075401 (2020).

[19] D. Golde, T. Meier, and S. W. Koch, Phys. Rev. B **77**, 075330 (2008).

[20] T. T. Luu and H. J. Wörner, Phys. Rev. B **94**, 115164 (2016).

[21] H. Haug and S. W. Koch, *Quantum Theory of the Optical and Electronic Properties of Semiconductors*, 5th ed. (World Scientific, Singapore, 2009).

[22] Z. W. Wang, S. C. Jiang, G. L. Yuan, T. Wu, C. Li, C. Qian, C. Jin, C. Yu, W. J. Hua, and R. F. Lu, Sci. China Phys. Mech. Astron. **63**, 257311 (2020).

[23] L. Li, P. Lan, X. Zhu, T. Huang, Q. Zhang, M. Lein, and P. Lu, Phys. Rev. Lett. **122**, 193901 (2019).

[24] S. C. Jiang, S. Gholam-Mirzaei, E. Crites, J. E. Beetar, M. Singh, R. F. Lu, M. Chini, and C. D. Lin, J. Phys. B **52**, 225601 (2019).

[25] T. J. Shao, L. J. Lu, J. Q. Liu, and X. B. Bian, Phys. Rev. A **101**, 053421 (2020).

[26] G. Vampa, C. R. McDonald, G. Orlando, P. B. Corkum, and T. Brabec, Phys. Rev. B **91**, 064302 (2015).

[27] L. Meckbach, T. Stroucken, and S. W. Koch, Phys. Rev. B **97**, 035425 (2018).

[28] C. Yu, S. C. Jiang, and R. F. Lu, Adv. Phys. X **4**, 1562982 (2019).

[29] M. V. Berry, Proc. R. Soc. London, Ser. A **392**, 45 (1984).

[30] Y. S. You, M. Wu, Y. Yin, A. Chew, X. Ren, S. Gholam-Mirzaei, D. A. Browne, M. Chini, Z. Chang, K. J. Schafer, M. B. Gaarde, and S. Ghimire, Opt. Lett. **42**, 1816 (2017).

[31] J. Li, X. Zhang, S. Fu, Y. Feng, B. Hu, and H. Du, Phys. Rev. A **100**, 043404 (2019).

[32] L. Yue and M. B. Gaarde, Phys. Rev. Lett. **124**, 153204 (2020).

[33] C. Yu, X. R. Zhang, S. C. Jiang, X. Cao, G. L. Yuan, T. Wu, L. H. Bai, and R. F. Lu, Phys. Rev. A **94**, 013846 (2016).

[34] S. C. Jiang, J. G. Chen, H. Wei, C. Yu, R. F. Lu, and C. D. Lin, Phys. Rev. Lett. **120**, 253201 (2018).

[35] K. S. Virk and J. E. Sipe, Phys. Rev. B **76**, 035213 (2007).

[36] R. W. Nunes and X. Gonze, Phys. Rev. B **63**, 155107 (2001).

[37] I. Souza, J. Íñiguez, and D. Vanderbilt, Phys. Rev. B **69**, 085106 (2004).

[38] U. Lindefelt, H. E. Nilsson, and M. Hjelm, Semicond. Sci. Technol. **19**, 1061 (2004).

[39] N. Marzari, A. A. Mostofi, J. R. Yates, I. Souza, and D. Vanderbilt, Rev. Mod. Phys. **84**, 1419 (2012).

[40] R. Sakuma, Phys. Rev. B **87**, 235109 (2013).

[41] G. Pizzi, V. Vitale, R. Arita, S. Blügel, F. Freimuth, G. Géranton, M. Gibertini, D. Gresch, C. Johnson, T. Koretsune *et al.*, J. Phys.: Condens. Matter **32**, 165902 (2020).

[42] R. E. F. Silva, F. Martin, and M. Ivanov, Phys. Rev. B **100**, 195201 (2019).

[43] N. Tancogne-Dejean, M. A. Sentef, and A. Rubio, Phys. Rev. Lett. **121**, 097402 (2018).

[44] C. Yu, S. C. Jiang, T. Wu, G. L. Yuan, Y. G. Peng, C. Jin, and R. F. Lu, arXiv:2006.00861.

[45] V. S. Yakovlev and M. S. Wismer, Comput. Phys. Commun. **217**, 82 (2017).

[46] J. Zak, Phys. Rev. Lett. **62**, 2747 (1989).

[47] M. Du, C. Liu, Y. Zheng, Z. Zeng, and R. Li, Phys. Rev. A **100**, 043840 (2019).

[48] R. Resta, J. Phys.: Condens. Matter **12**, R107 (2000).

[49] G. Kresse and J. Hafner, Phys. Rev. B **47**, 558 (1993).

[50] N. Tancogne-Dejean, O. D. Muecke, and F. X. Kaertner, Nat. Commun. **8**, 745 (2017).

[51] Y. S. You, D. A. Reis, and S. Ghimire, Nat. Phys. **13**, 345 (2017).

[52] Y. S. You, J. Lu, E. F. Cunningham, C. Roedel, and S. Ghimire, Opt. Lett. **44**, 530 (2019).

[53] Y. T. Zhao, X. Q. Xu, S. C. Jiang, X. Zhao, J. G. Chen, and Y. J. Yang, Phys. Rev. A **101**, 033413 (2020).